

## Relaxation time as early warning signal of avalanches in self-organizing systems

Zhiqin Ma<sup>1</sup>, Chunhua Zeng<sup>1,\*</sup> and Wu-Ming Liu<sup>2,3,4,†</sup>

<sup>1</sup>Faculty of Science, Kunming University of Science and Technology, Kunming 650500, China

<sup>2</sup>Beijing National Laboratory for Condensed Matter Physics, Institute of Physics, Chinese Academy of Sciences, Beijing 100190, China

<sup>3</sup>School of Physical Sciences, University of Chinese Academy of Sciences, Beijing 100190, China

<sup>4</sup>Songshan Lake Materials Laboratory, Dongguan, Guangdong 523808, China



(Received 9 July 2023; accepted 20 November 2023; published 4 January 2024)

Avalanches are sudden, destructive, and extremely difficult to forecast natural disasters that can result in numerous fatalities and extensive property damage. Given the immense danger posed by avalanches, there is a significant amount of attention paid to accurately predicting these events. We investigate the predictability of large avalanches in a class of self-organizing systems, which change their internal structure or function in response to external circumstances by manipulating or organizing other elements of the same system. Here, we propose a practical relaxation time to replace a traditional recovery time, and importantly, the relaxation time does not require the removal of part of the resources (perturb state variables) in the environment. This work provides examples of the forest fire model and sandpile model as self-organizing systems in which the relaxation time successfully predicts the onset of large avalanches. Furthermore, the relaxation time can show a consistent with the increasing trend in both oscillatory and nonoscillatory bifurcations, suggesting that the relaxation time is more universal than traditional indirect metrics such as the variance and the lag-1 autocorrelation function. We aim to identify early warning signals before the onset of large avalanches and provide scientific evidence and significant information for managers to formulate mitigation countermeasures and strategic decisions.

DOI: [10.1103/PhysRevResearch.6.013013](https://doi.org/10.1103/PhysRevResearch.6.013013)

### I. INTRODUCTION

The dynamics of self-organizing systems [1–10] in nature often occur in terms of catastrophic shifts [11–16] or avalanches [17–19]. Avalanche events are increasingly attracting the attention of scientists and decision makers since of their impact on ecosystems, which is exacerbated by our increasing global environmental degradation [8,20]. Examples of avalanches include forest fires [21–23], landslides [24–27], earthquakes [28–30], solar flares [31–33], and neuronal activity [34,35]. Avalanches are natural disasters that are sudden, destructive, and extremely difficult to forecast, and can cause a large number of casualties and heavy property losses [36–39]. Due to the potential hazards posed by avalanches, there is a significant amount of attention paid to predicting these events.

Systems with self-organized criticality [40–47] properties can spontaneously evolve to a critical state in which small changes trigger major avalanches due to subtle interdependencies between elements [48,49]. The conjecture of avalanche events with self-organized criticality leads to an adverse recommendation to efforts of a class of self-organizing systems

prediction. This is because self-organized criticality means that it is difficult to predict where and when an avalanche will occur and how strong it will become [50–55]. Understanding the self-organizing behavior of systems under changing environmental conditions and improving capabilities to predict large avalanches are priorities for research [56,57]. An influential approach to predicting the onset of large avalanches is to estimate changes in the critical exponent, and good results have been obtained [58–65]. Despite its appeal, the critical exponent in fact has a limitation: The results of the critical exponent usually require high-resolution spatial data, and such data are sometimes not available [60,66–68].

Both theoretical and experimental studies have shown that the recovery rate from perturbation should go to zero as the system approaches a tipping point, and this is the essence of critical slowing down [69–71]. Much work has been focused on ways to infer critical slowing down from indirect indicators such as variance [72–74] and lag-1 autocorrelation [75–77]. Although these indicators are associated with critical slowing down in simple stochastically forced models [8,74,78], the indirect indicators do not always respond in a simple way [79]. It has been confirmed by experiments that trends in indirect indicators emerged in the climate [8], the food web of a lake [80], and laboratory populations of water fleas [7] systems, but were not all consistent. The simplest way to measure the close to a tipping point would be to directly measure the recovery time at which the system state returns to its initial equilibrium state after a perturbation [81,82]. A perturbation experiment (recovery time) is the most direct way to measure critical slowing down and may be more informative than other

\*zch2009@126.com

†wliu@iphy.ac.cn

Published by the American Physical Society under the terms of the [Creative Commons Attribution 4.0 International](https://creativecommons.org/licenses/by/4.0/) license. Further distribution of this work must maintain attribution to the author(s) and the published article's title, journal citation, and DOI.

warning signals in some cases [9,70]. However, they may be difficult to implement both for practical and conceptual reasons. Not only it is difficult to remove a part of the biomass of a population, but such perturbation may potentially trigger itself a transition if it pushes the state of the system beyond its present basin of attraction [9,11,83]. How to measure critical slowing down, while it does not remove part of the resources (perturb state variables) in the environment, is a difficult problem that we urgently need to solve.

In this paper, we propose a practical relaxation time (relaxation rate) to replace a traditional recovery time (recovery rate). Importantly, the advantage of applying the relaxation time indicator is that it does not require the removing of part of the resources (perturb state variables) in the environment. This work provides examples of the forest fire model and the sandpile model as self-organizing systems where the lag- $\tau$  autocorrelation function was calculated by extracting low-resolution time series data in the simulation. Then, the lag- $\tau$  autocorrelation function is fitted by the damped sine wave function to obtain the relaxation time. Therefore, the relaxation time can be a practical indicator to predict a class of self-organizing systems and provides a viable perspective to predict avalanche events.

The paper is organized as follows. In Sec. II A, we present detailed expressions for the predictive indicators. In Sec. II B, we propose a practical relaxation time (relaxation rate) to replace a traditional recovery time (recovery rate). In Sec. III, we describe the details of the forest fire model and the sandpile model. In Sec. IV, we apply the relaxation time, relaxation rate, variance, and lag- $\tau$  autocorrelation indicators to identify the onset of large avalanches in self-organizing systems (i.e., forest fire and sandpile model). In Sec. V, we develop strategies to prevent avalanches in forest fires. Finally, in Sec. VI, we discuss our results and draw conclusions.

## II. METHODS

### A. Indicators

Critical slowing down can give rise to larger fluctuations near the equilibrium state of the system, which leads to an increase in the variance of the system prior to the transitions. The variance of the state variable is defined as [74,79]:

$$\sigma^2 = \frac{1}{M} \sum_{t=1}^M (\rho(t) - \mu)^2, \quad (1)$$

where  $M$  denotes the rolling window sizes,  $\rho(t)$  is the state variable density at time  $t$ , and  $\mu$  is the mean.

The lag- $\tau$  autocorrelation function is the correlation between values that are  $\tau$  time periods apart. The lag- $\tau$  autocorrelation function  $ACF(\tau)$  can be calculated by the following relation [8,78,84]:

$$ACF(\tau) = \frac{E[(\rho(t) - \mu)(\rho(t + \tau) - \mu)]}{\sigma^2}, \quad (2)$$

where  $\tau$  is the lag time and  $E[\dots]$  denotes the mathematic expectation.

The lag- $\tau$  autocorrelation function is fitted by the following damped sine wave function [15,85,86]:

$$ACF(\tau) = A \exp\left(-\frac{\tau}{T}\right) \sin\left(\pi \frac{\tau - \tau_c}{\omega}\right) + y_0, \quad (3)$$

where  $T$  is the relaxation time, defined as the time required to recover from the unstable to the stable state.  $A$ ,  $\tau_c$ ,  $\omega$ , and  $y_0$  are amplitude, phase shift, period, and offset, respectively.

The relaxation rate ( $\lambda$ ) can be used as an indicator of whether a system is getting close to the tipping points [9,70,82]. The relaxation rate is similar to the concept of the recovery rate and is defined as the reciprocal of the relaxation time ( $T$ ), i.e.,

$$\lambda = 1/T. \quad (4)$$

### B. Theory of critical slowing down

We illustrate the theory of critical slowing down using a well-known plant population model [87]:

$$\frac{dX}{dt} = rX \left(1 - \frac{X}{K}\right) - \gamma \frac{X^2}{X^2 + a^2} + \xi(t), \quad (5)$$

where  $X$  is population density,  $r$  is the growth rate (set to 1.0),  $K$  is the carrying capacity (set to 10),  $\gamma$  is the maximum grazing rate (set to 2.45 for high resilience and 2.60 for low resilience),  $a$  is the efficiency of the grazer (set to 1.6), and  $\xi(t)$  is the Gaussian white noise defined as  $\langle \xi(t) \rangle = 0$  and  $\langle \xi(t)\xi(t') \rangle = 2\sigma\delta(t - t')$ , in which  $\sigma$  is the noise intensity (set to 0.1). The panel in Fig. 1(a) shows stable (solid lines) and unstable (dashed lines) equilibria for different grazing rates. The grey dotted arrows in the figure show that stable equilibria are attracting, while unstable equilibria are repelling. We refer to an equilibrium as stable if the system tends to return to it after experiencing small perturbations or fluctuations. Conversely, an equilibrium is considered unstable if the system does not return to it after such perturbations.

Understanding whether a system is approaching a tipping point will be of great practical importance. The resilience of a system is defined as the magnitude of perturbation that the system can withstand without falling into an alternative state [83,88]. A system in a stable state with high resilience [see Fig. 1(b)] and one with low resilience [see Fig. 1(c)] are compared by the so-called ‘‘ball-in-a-cup’’ diagram. The ball denotes the state of the system, which moves towards a stable equilibrium with a velocity proportional to the steepness of the basin of attraction (yellow area). In Fig. 1(b), a perturbation would need to be quite strong to push the high-resilience system from its stable state  $X = 6.22$  to the other stable state at  $X = 1.51$ . In contrast, the ‘‘ball-in-a-cup’’ diagram in Fig. 1(c) illustrates that a smaller push is required for the low-resilience system to transition from  $X = 5.55$  to  $X = 1.37$ . Therefore, the system with lower resilience is closer to the tipping point. However, without a realistic mathematical model to evaluate the impact of perturbations of different magnitudes, it becomes difficult to employ resilience as an indicator for detecting critical transitions.

The stability of the system provides a more practical way of assessing whether the system is approaching a tipping point. Stability is defined as the time that it takes for the system state

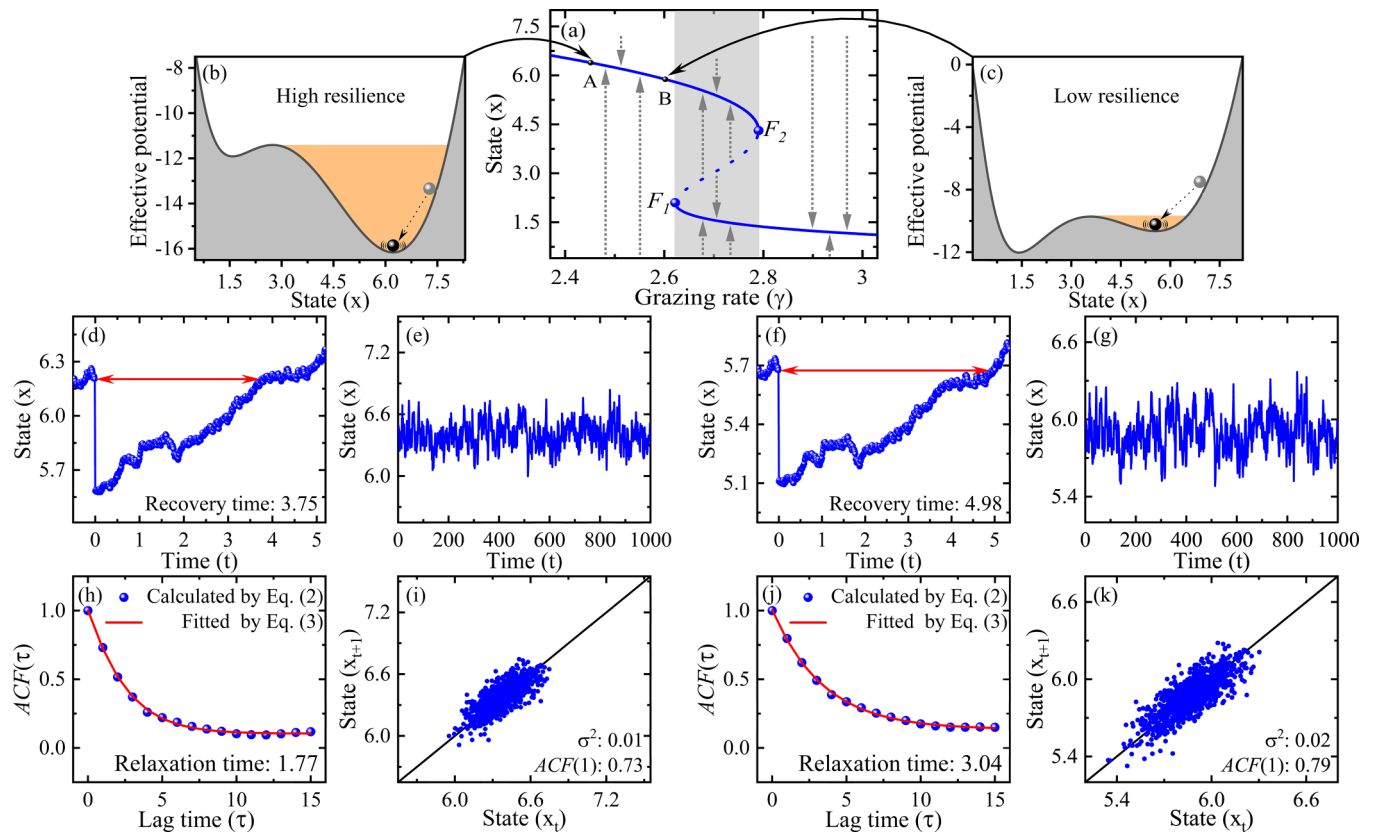


FIG. 1. As a system approaches a catastrophic bifurcation (such as  $F_1$  or  $F_2$ ), there are some characteristic changes in the nonequilibrium dynamics. (a) shows the change in stable (solid lines) and unstable (dashed lines) equilibria as the grazing rate changes. (b) and (c) show the effective potential landscape of the system for different grazing rates. Critical slowing down as an indicator that the system has lost resilience and may therefore be tipped more easily into an alternative state. Recovery rates upon small perturbations [(d) and (f)] are slower if the basin of attraction is small (c) than when the basin of attraction is larger (b). Red arrow width represents the time it takes for the system state to return to its initial state after a perturbation (10% reduction in resources), which is called the recovery time. The effect of this critical slowing down may be measured in stochastically induced fluctuations in the system state [(e) and (g)] as increased relaxation time [(h) and (j)], variance and lag-1 autocorrelation function [(i) and (k)].

to return to its equilibrium state following a small external perturbation [9,89]. As depicted in Fig. 1(a), systems with higher resilience possess larger and deeper basins of attraction in their landscapes, allowing them to recover more quickly from small perturbations than systems with lower resilience. The systems with higher resilience have a faster recovery time of 3.75 units, as shown in Fig. 1(d). In contrast, the systems with lower resilience have a slower recovery time of 4.98 units, as shown in Fig. 1(f). This phenomenon is known as critical slowing down [10,69–71], where the recovery time should increase (or the recovery rate should decrease) as the system approaches a tipping point.

Figures 1(e) and 1(g) show a simulated time-series subject to noise for a system with higher resilience (left) and lower resilience (right). There is evidence that certain characteristic changes in the pattern of fluctuations are expected to occur when approaching a bifurcation in such systems [6,90–92]. Because critical slowing down leads to a decrease in the intrinsic rates of change of the system, the state of the system at any given moment becomes more and more like its past state. The resulting increase in “memory” of the system can be measured from the lag- $\tau$  autocorrelation function of the system [78,93–95]. We then fit the lag- $\tau$  autocorrelation function with

a damped sine wave function to finally obtain the relaxation time. Relaxation time is defined as the time required to recover from the unstable to the stable state, and its definition is similar to the concept of stability. In Figs. 1(h) and 1(j), the more resilient systems have a shorter relaxation time (1.77 units), while the less resilient systems have a longer relaxation time (3.04 units). Near the tipping point, the relaxation time and the traditional recovery time increase simultaneously [see Figs. 1(f) and 1(j)]. It can be seen that the relaxation time is proportional to the traditional recovery time. This means that we could use the relaxation time (relaxation rate) to replace the traditional recovery time (recovery rate), and importantly the relaxation time does not require the removing part of the resources (perturb state variables) in the environment. Critical slowing down leads to system states becoming more similar to each other, which is reflected as an increase in lag-1 autocorrelation [see Figs. 1(i) and 1(k)]. Similarly, since systems with lower resilience are slower to return to equilibrium, the external perturbations may accumulate and push the system further away from equilibrium, resulting in an increase in variance [see Figs. 1(i) and 1(k)]. In summary, the phenomenon of critical slowing down leads to these possible early warning signals in the dynamics of a system approaching

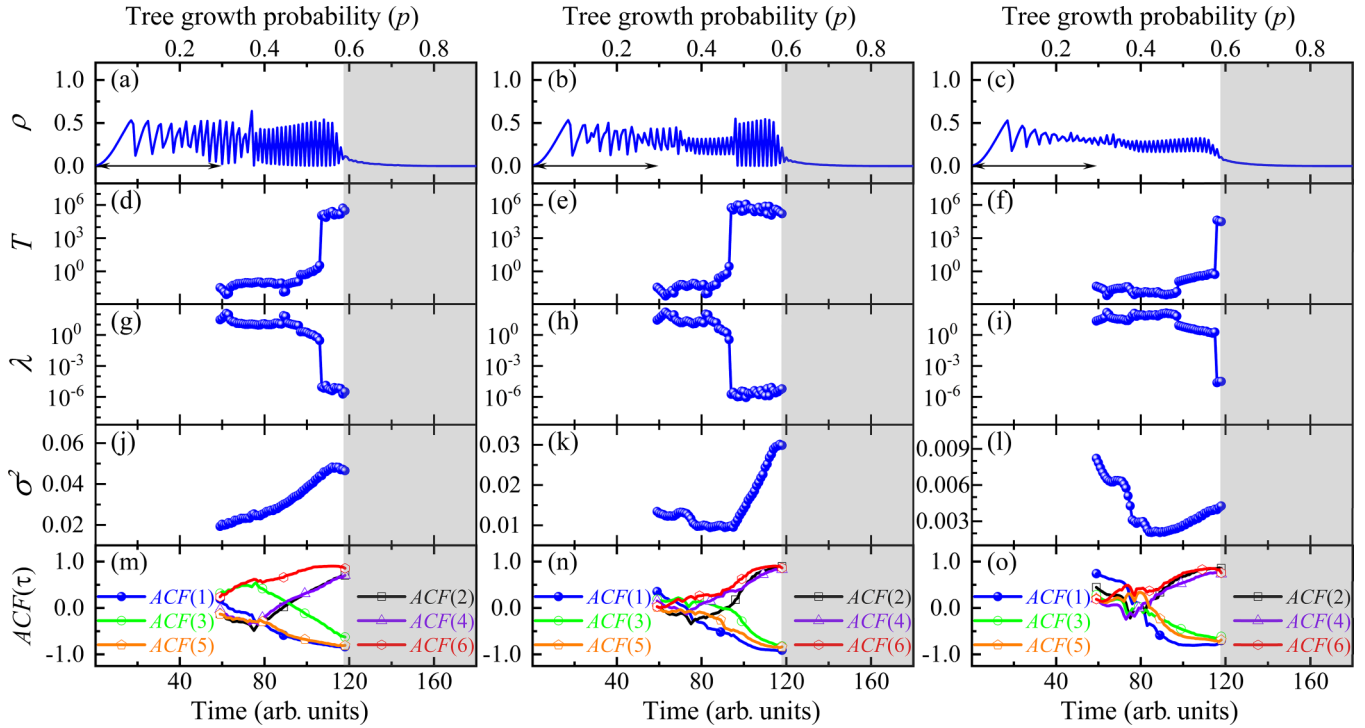


FIG. 2. Trends in indicators preceding to large avalanches for the forest fire model with system sizes (the first column)  $L^2 = 256 \times 256$ , (the second column)  $L^2 = 512 \times 512$ , and (the third column)  $L^2 = 1024 \times 1024$ . [(a)–(c)] Transient time series for the tree density  $\rho(t)$ . Arrow illustrates the rolling window (50% of the time series) used for computing early warning signals. [(d)–(f)] Relaxation time provides an increasing trend in the three different system sizes. [(g)–(i)] Relaxation rate goes to zero as the system approaches large avalanches. [(j)–(l)] Variance gives an early warning signal, but with a weaker rising trend than relaxation time. [(m)–(o)] The trend of lag- $\tau$  autocorrelation function depends on the lag time. When lag time is an odd number [see blue sphere, green circle, and orange pentagon in (m)–(o)], it will be a decreasing trend, while when lag time is an even number [see black square, purple triangle, and red hexagon in (m)–(o)], it will be an increasing trend. Note that tipping point was determined by the theoretical percolation threshold  $p_c \approx 0.593$ . The  $p$  increases linearly by 0.005 for each time step in the range  $0.005 \leq p \leq 0.900$ . The grey band identifies the state after large avalanches and the parameter of the tipping point is Time = 118.

a bifurcation: increased relaxation time (or decreased relaxation rate), increased recovery time (or decreased recovery rate), increased variance and increased lag-1 autocorrelation function.

### III. SELF-ORGANIZING SYSTEMS

#### A. Forest fire model

We considered that the time scales of tree growth and burning down of tree clusters are separated [21,23,59]. Burning trees evolve on a fast time scale, whereas trees grow on a slow time scale [96]. In other words, burning trees can burn the entire cluster of trees in days to months, so they have a maximum time scale of months. In contrast, trees take up to decades to grow into a dense forest. Here, we investigate a stochastic forest fire model that evolves in continuous time. Each cell on a  $L \times L$  square lattice is either empty or occupied by a tree. The state of the system is updated by three dynamical rules: (i) At an empty cell, a tree grows with probability  $p$ . (ii) Lightning strikes each cell with probability  $k \ll p$ , followed by instantaneously burning the entire nearest neighbor cluster if that cell has trees. Note that we use the von Neumann neighborhood. (iii) All burning trees become empty

cells. The tree growth probability  $p$  increases linearly over the interval  $[0.005, 0.900]$ , resulting in the avalanches. After each stepwise change in the control parameter, the tree density  $\rho$  of the lattice is stored for calculation.

To avoid limited scale effects, the number of cells  $L \times L$  must be chosen to be much larger than the maximum cluster of trees. Various system sizes between 128 to 1024 ( $L = 128, 256, 512$ , and 1024) are screened. For a real wildfire model in ecology, the size of the cells should be approximately between 6 and 55 ha [23,97], so that each “tree” actually describes the behavior of a larger forest. Therefore, a simulation with  $L = 1024$  can represent a forest of up to 512 000 km<sup>2</sup> [23]. In our simulations, we assume that tree growth probability  $p$  is between 0.005 to 0.900, and lightning strike probability  $k$  is 0.0001.

#### B. Sandpile model

We consider the two-dimensional sandpile model on a square lattice of size  $L \times L$ , where integer variables  $z(x, y) \geq 0$  represent local energies [46,98–100]. One perturbs the system by adding grains at the central site according to

$$z(x, y) \mapsto z(x, y) + 1. \quad (6)$$

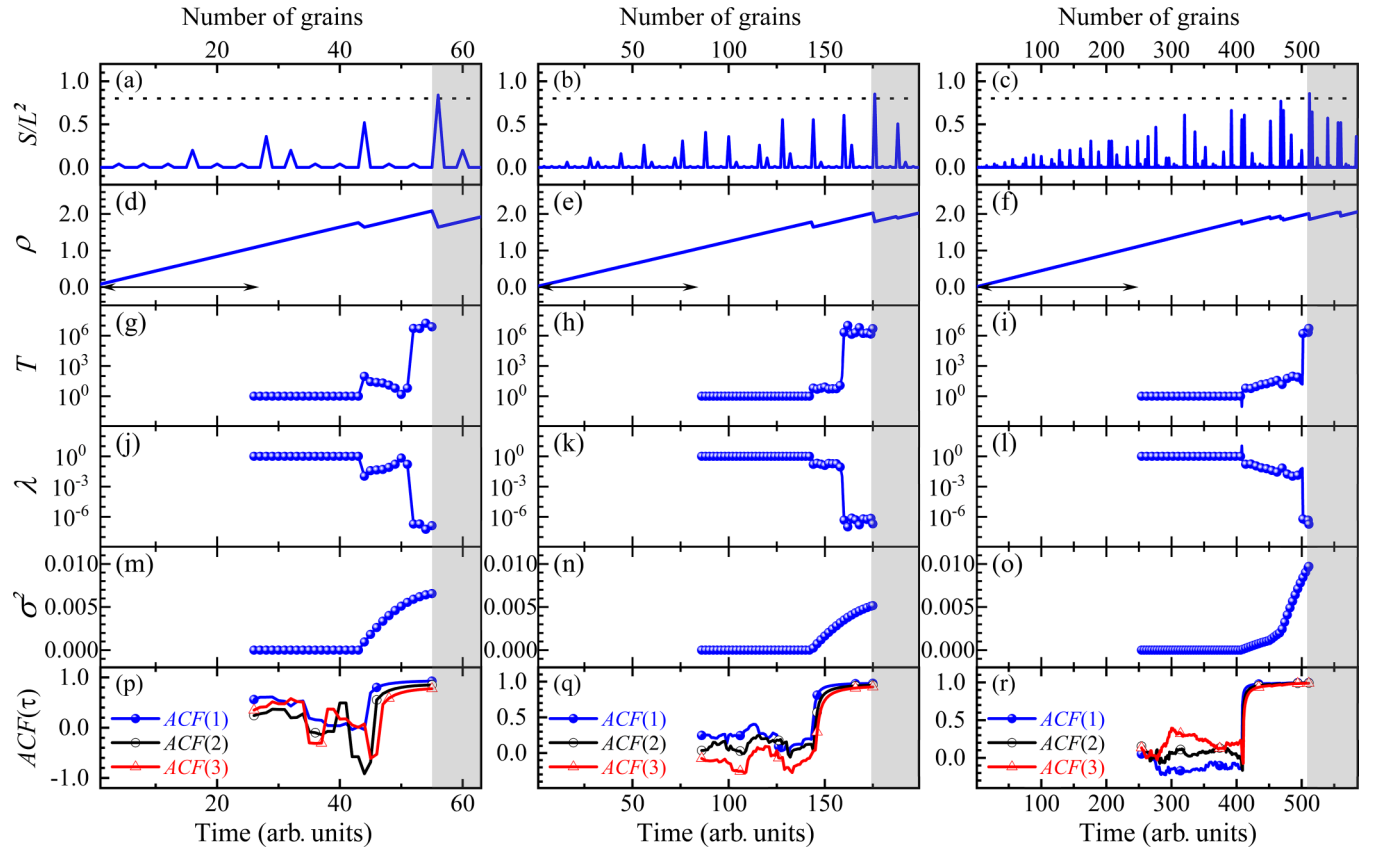


FIG. 3. Trends in indicators prior to large avalanches for the sandpile model with system sizes (the first column)  $L^2 = 5 \times 5$ , (the second column)  $L^2 = 9 \times 9$ , and (the third column)  $L^2 = 15 \times 15$ . [(a)–(c)] Normalized avalanche size as a function of the number of grains and time. The horizontal dashed lines in (a)–(c) indicate the large avalanches  $S/L^2 \geq 0.8$ . [(d)–(f)] Time series for the average sandpile density  $\rho(t)$ . Arrow illustrates the rolling window (50% of the time series) used for computing early warning signals. [(g)–(i)] Relaxation time provides an increasing trend in the three different system sizes. [(j)–(l)] Relaxation rate goes to zero as the system approaches large avalanches. [(m)–(o)] Variance gives an early warning signal, but with a weaker rising trend than relaxation time. [(p)–(r)] The lag- $\tau$  autocorrelation function also has an increasing trend, which is consistent with the variance. The number of grains increases linearly by 1.0 for each time step. The grey band identifies the state after large avalanches, and the parameters of the tipping point are Time = 56 (the first column), Time = 176 (the second column), and Time = 512 (the third column).

Our model is a cellular automaton that describes the interactions of an integer variable with its nearest neighbors. In two-dimensions,  $z(x, y)$  is updated synchronously as follows:

$$z(x, y) \rightarrow z(x, y) - h_c, \quad (7)$$

$$z(x \pm 1, y) \rightarrow z(x \pm 1, y) + 1, \quad (8)$$

$$z(x, y \pm 1) \rightarrow z(x, y \pm 1) + 1. \quad (9)$$

if  $z(x, y)$  exceeds a critical value  $h_c$  (set to  $h_c = 4$  throughout this work). We assume open boundary conditions with energies fixed to zero at the boundary. The integer variables may be thought of as the local slope of the sandpile in some direction. If the slope is too steep, the sand slides, reducing the slope but increasing the slope for the neighbors. The system is set up with empty initial conditions  $z(x, y) = 0$ . It then evolves over time until avalanches occur. After each incremental increase in the number of grains, the avalanche size  $S$  and the average sandpile density  $\rho$  of the lattice are recorded for subsequent analysis.

#### IV. EARLY WARNING SIGNALS OF AVALANCHES

The tree density  $\rho$  is plotted versus the tree growth probability  $p$  for the three system sizes [see Figs. 2(a)–2(c)]. Arrow indicates the rolling window (50% time series for the tree density) used for computing early warning signals. At low tree growth probability  $p < p_c$ , the trajectories of the tree density  $\rho(t)$  indicate periodic oscillations. At the critical probability (percolation threshold  $p_c \approx 0.593$  [101–103]), the so-called spanning clusters (large avalanches) emerge and the sharp decrease of the tree density  $\rho$  is observed. When tree growth probability  $p$  is increased further, the tree density is approximately zero since more and more cells become part of the spanning clusters. Figures 2(d)–2(f) display the results of relaxation time for different system sizes. For the three system sizes  $L = 256, 512$ , and  $1024$ , the relaxation time significant increase by five orders of magnitude before the large avalanches. Therefore, the relaxation time would provide an effective approach to predict the onset of the large avalanches in self-organizing systems. In practice, the relaxation time may be difficult to apply for direct comparisons. Therefore,

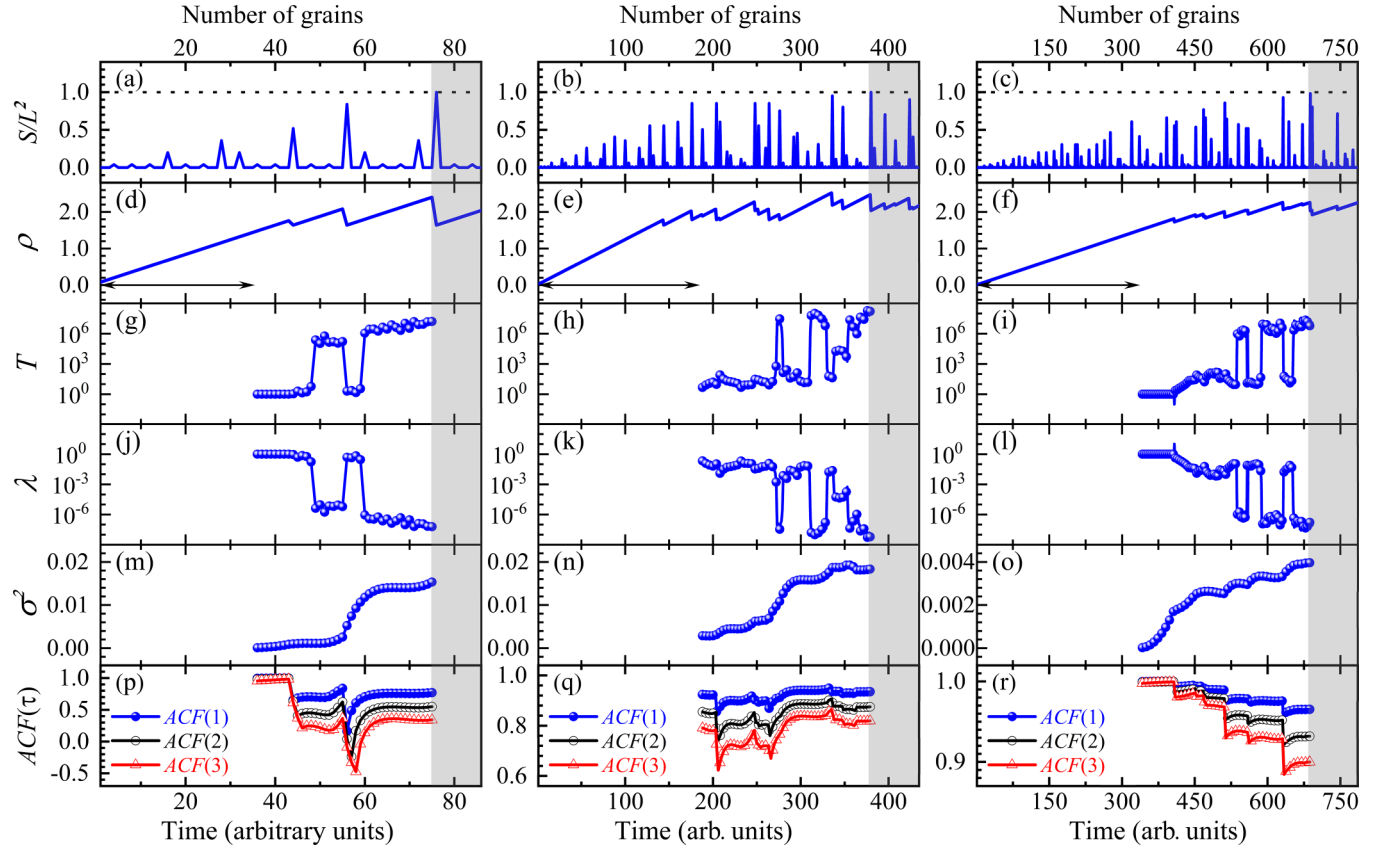


FIG. 4. Trends in indicators prior to the largest avalanches for the sandpile model with system sizes (the first column)  $L^2 = 5 \times 5$ , (the second column)  $L^2 = 9 \times 9$ , and (the third column)  $L^2 = 15 \times 15$ . [(a)–(c)] Normalized avalanche size as a function of the number of grains and time. The horizontal dashed lines in (a)–(c) indicate the largest avalanches  $S/L^2 \approx 1.0$ . [(d)–(f)] Time series for the average sandpile density  $\rho(t)$ . Arrow illustrates the rolling window (50% of the time series) used for computing early warning signals. [(g)–(i)] Relaxation time provides an increasing trend in the three different system sizes. [(j)–(l)] The relaxation rate goes to zero as the system approaches largest avalanches. [(m)–(o)] Variance gives an early warning signal, but with a weaker rising trend than relaxation time. [(p)–(r)] The lag-1, lag-2, and lag-3 autocorrelation function provide do not exhibit significant signals, but higher lag times produce larger trends. The number of grains increases linearly by 1.0 for each time step. The grey band identifies the state after largest avalanches, and the parameters of the tipping point are Time = 76 (the first column), Time = 380 (the second column), and Time = 688 (the third column).

the relaxation rate indicator would be more effective. In Figs. 2(g)–2(i), the relaxation rate goes to zero as the system approaches the large avalanches. In Figs. 2(j)–2(k), the variance also show the rising trend before the large avalanches. For larger systems [see Fig. 2(l)], unfortunately, the variance provides no useful signal due to the weak amplitude of the tree density quasiperiodic oscillations. In Figs. 2(m)–2(o), the lag- $\tau$  autocorrelation function  $ACF(\tau)$  displays the correlation between values that are  $\tau$  time periods apart. The autocorrelation function decreases at lag-1, lag-3, and lag-5, while it increases at lag-2, lag-4, and lag-6. This may be due to the fact that the forest fire model yields oscillations with a period 2. As a result, bifurcations with an oscillatory component yield an increasing or a decreasing trend, which depends on the relationship between the lag times and the period of oscillations. These show that the scheme of requiring increasing variance and lag-1 autocorrelation function to predict the onset of avalanches is not always useful. It also suggests that the autocorrelation function should be computed at multiple lag times and not just at lag-1.

Figures 3(a)–3(c) show how the normalized avalanche size varies with increasing grain number and time for the large avalanche. Note that here the large avalanche is defined as a normalized avalanche size equal to or greater than 0.8. The transient time series of average sandpile density for the three system sizes as shown in Figs. 3(d)–3(f). Arrow indicates the rolling window (50% time series for the average sandpile density) used for computing early warning signals. Figures 3(g)–3(i) show the relaxation time as a function of the number of grains and time. Obviously, the relaxation time shows a recognizable trend (significant increase) before the large avalanches occur. The relaxation rate, defined as the reciprocal of the relaxation time, is close to zero as the system approaches an avalanche [see Figs. 3(j)–3(l)]. As gradually increasing the number of grains brings the self-organizing system to the tipping point spontaneously, the external perturbations may accumulate which leads to an increase in variance [see Figs. 3(m)–3(o)]. The lag-1, lag-2, and lag-3 autocorrelation functions show increasing trends for different system sizes, with more significant trends at higher lag times

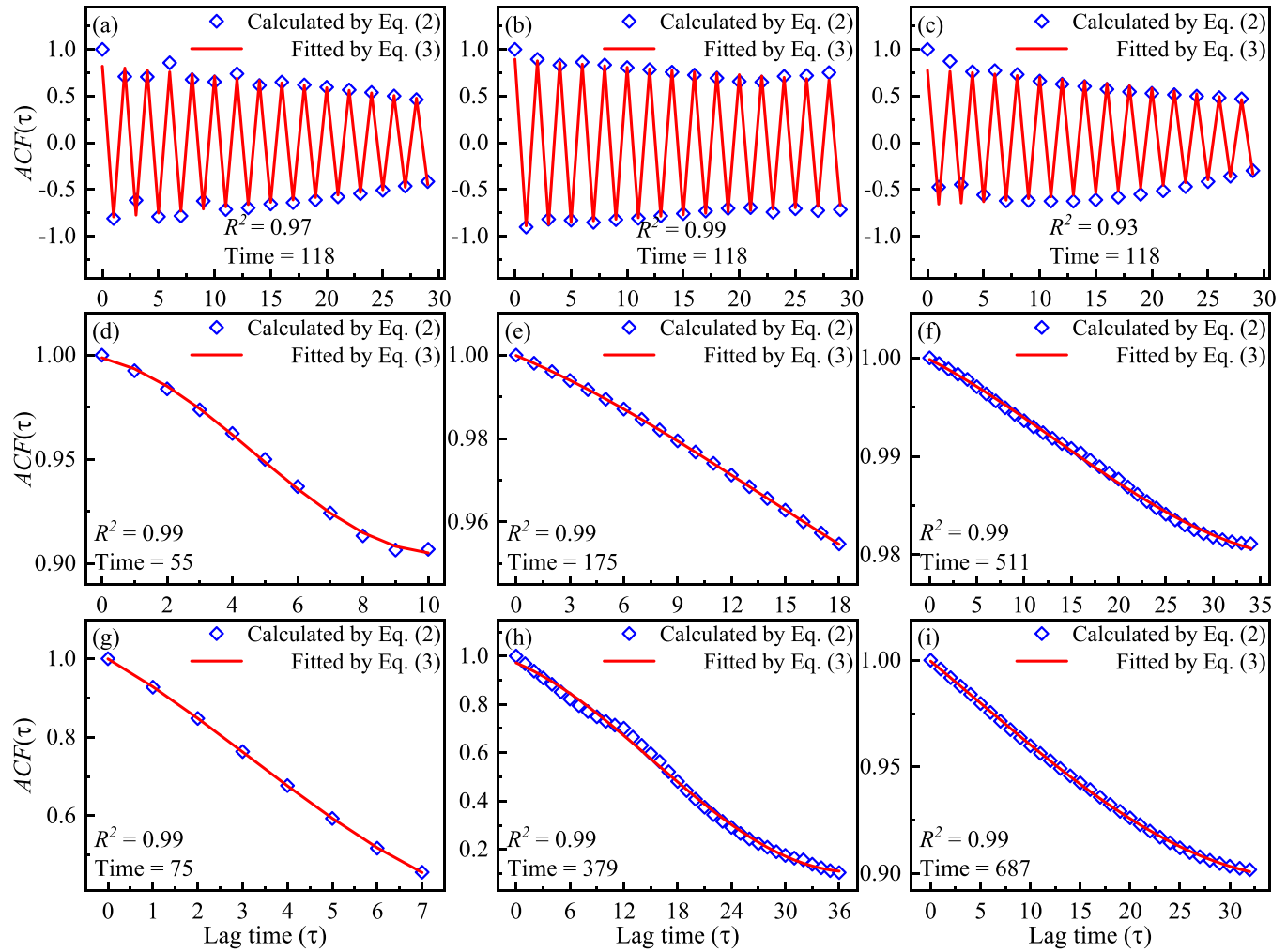


FIG. 5. The lag- $\tau$  autocorrelation function for the forest fire model with system sizes (a)  $L^2 = 256 \times 256$ , (b)  $L^2 = 512 \times 512$ , and (c)  $L^2 = 1024 \times 1024$  and the sandpile model with system sizes [(d) and (g)]  $L^2 = 5 \times 5$ , [(e) and (h)]  $L^2 = 9 \times 9$ , and [(f) and (i)]  $L^2 = 15 \times 15$ . [(a)–(c)] Autocorrelation function of tree density as functions of lag time (blue diamonds). [(d)–(f)] Autocorrelation function of average sandpile density as functions of lag time (blue diamonds) in the largest avalanches. [(g)–(i)] Autocorrelation function of average sandpile density as functions of lag time (blue diamonds) in the largest avalanches. The red solid lines correspond to fitted curves of the damped sine wave function of the form  $A \exp(-\tau/T) \sin[\pi(\tau - \tau_c)/\omega] + y_0$ , where  $A$ ,  $T$ ,  $\tau_c$ ,  $\omega$ , and  $y_0$  are used as the free fitting parameters. The closer coefficient of determination ( $R^2$ ) is to 1.0, and the fitting degree of the indicator is better.

[see Figs. 3(p)–3(r)]. This suggests that the autocorrelation function should be calculated at multiple lag times and may provide a more accurate early warning signal.

To compare the performance of early warning signals under different avalanche sizes, we studied not only the indicator trends before the large avalanches [see Fig. 3] but also those before the largest avalanche [see Fig. 4]. Figures 4(a)–4(c) show how the avalanche size varies with increasing grain number and time for the largest avalanche. Note that here the largest avalanche is defined as a normalized avalanche size approximately equal to 1.0. In Figs. 4(d)–4(f), we used longer transient time series of average sandpile density for the three system sizes. Arrow indicates the rolling window (50% time series for the average sandpile density) used for computing early warning signals. The relaxation time [see Figs. 4(g)–4(i)], relaxation rate [see Figs. 4(j)–4(l)], variance [see Figs. 4(m)–4(o)], and lag- $\tau$  autocorrelation function [see Figs. 4(p)–4(r)] indicators are calculated separately for

comparison with corresponding indicators in Fig. 3. In the scenario undergoing the largest avalanche [Figs. 4(g)–4(r)], the trajectory shows a strong increasing (decreasing) trend in relaxation time (relaxation rate) and variance, but no discernible trend in the lag-1, lag-2, and lag-3 autocorrelation function. Therefore, the protocol of requiring increasing the variance and the autocorrelation function of lower lag time to represent the early warning signal fails in this case. Fortunately, since the relaxation time is obtained by fitting the autocorrelation function at multiple lag times, it still provides an early warning signal prior to the large avalanches. According to this criterion, the relaxation time (relaxation rate) is a more sensitive and robust indicator than lag- $\tau$  autocorrelation function.

In Figs. 5, we show the lag- $\tau$  autocorrelation function for different system sizes at a moment before the avalanche. We find excellent agreement (coefficient of determination [104,105]:  $R^2 > 0.9$ ) between the numerical (blue diamond

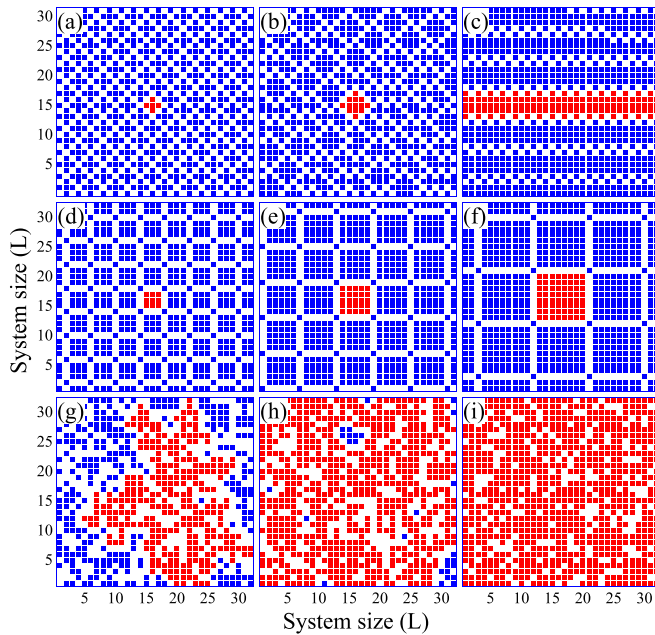


FIG. 6. These spatial snapshots correspond to the different growth patterns. [(a)–(c)] Diamond, [(d)–(f)] square, and [(g)–(i)] random growth patterns (protection strategies) for different tree densities (the first column)  $\rho = 0.60$ , (the second column)  $\rho = 0.70$ , and (the third column)  $\rho = 0.80$  (living trees, empty cells, and burning trees are shown in blue, white, and red, respectively). Burning area (red) is 0.488% (a), 1.270% (b), and 12.500% (c) in the first rows, 0.888% (d), 2.441% (e), and 6.250% (f) in the second rows, and 29.785% (g), 65.820% (h), and 79.785% (i) in the bottom rows, respectively. Compared with the burning area (maximum cluster size) of the random growth patterns, those for the best growth patterns (i.e., diamond or square protection strategies) are several orders of magnitude smaller. The system size is chosen for  $L^2 = 32 \times 32$ , which can represent a forest of up to 16 000 km<sup>2</sup> [23].

symbols) and fitting (red solid lines) results, which allows us to extract a relaxation time  $T$  explicitly. It means that the lag- $\tau$  autocorrelation function with either oscillations of period 2 [see Figs. 5(a)–5(c)] or exponential decay [see Figs. 5(d)–5(i)] could both be well fitted by the damped sine wave function.

## V. PREVENTION OF AVALANCHES IN FOREST FIRE

In Fig. 6, we show the spatial snapshots of diamond, square, and random growth patterns. The diamond growth pattern is more suitable than a square growth pattern in the presence of small tree densities  $\rho \lesssim 0.70$ . Conversely, the square growth pattern is more suitable for greater tree densities  $\rho \gtrsim 0.70$ . This means that we can choose different growth patterns (protection strategies) depending on the tree density when the signal is activated. For instance, the construction of biological fire forest belts and road engineering can prevent the onset of avalanches by dividing a large forest area into an optimal number of smaller areas.

We provide three different conservation strategies for the prevention of avalanches. A diamond growth pattern is a local optimal tiling, i.e., occupying empty cells on the basal plane (tree density  $\rho = 0.5$  and maximum cluster size  $S_{\max} = 1$ ) and

less than or equal to the set burning area (maximum cluster size). A square growth pattern is a simple square tiling, and a linear growth pattern is a simple linear tiling. Table I presents the diamond, square, and linear growth patterns compared to each other. For  $S_{\max} \lesssim 16$ , the diamond growth pattern is the best choice among the three growth patterns. However, when  $S_{\max} \gtrsim 25$ , the best growth pattern becomes the square growth pattern. These findings suggest that a diamond growth pattern is more suitable than a square growth pattern in the presence of the small burning area (maximum cluster sizes:  $S_{\max} \lesssim 16$ ). Conversely, the square growth pattern is more suitable for a greater burning area (maximum cluster sizes:  $S_{\max} \gtrsim 25$ ). A major limitation of a small burning area is tree densities less than 0.70. In addition, there is no limitation for a greater burning area. The same results are observed for the three system sizes ( $L = 128, 256, 512$ ), which implies that there are no scale effects in our growth patterns.

Table II shows the results on diamond, square, linear, and random growth patterns, and the best result in each block is in bold. Compared with the burning area of the random growth patterns, those for the best growth patterns are several orders of magnitude smaller. Moreover, when the tree density  $\rho \approx 0.6$ , it will lead to an increase in the burning area by two orders of magnitude, especially for the random growth pattern. This is because most cells form a dense spanning cluster, as previously noted. Our aim is to provide scientific evidence and significant information for managers to formulate mitigation countermeasures and strategic decisions prior to the onset of avalanches.

## VI. DISCUSSION

How to measure critical slowing down, while it does not remove part of the resources (perturb state variables) in the environment, is a challenging problem that we urgently need to solve. In this work, a relaxation time is proposed to identify the onset of large avalanches in self-organizing systems. The advantage of using the relaxation time indicator is that it does not require the removal of part of the resources (perturb state variables) in the environment, since the relaxation time is determined by fitting the lag- $\tau$  autocorrelation function. In practice, it is not easy to make direct comparisons by using relaxation time. Therefore, the relaxation rate indicator would be a more effective measure and could be used as an indicator of whether the system is close to a tipping point. The system is close to a tipping point the relaxation time should increase (or the relaxation rate should decrease), and this is the essence of critical slowing down. This work shows that relaxation rate is an excellent way to measure critical slowing down. Furthermore, relaxation time and relaxation rate offer complementary information to indirect indicators (such as variance and lag-1 autocorrelation) and should be added to the repertoire of tools for predicting tipping points in real systems.

The findings from Ref. [72] demonstrate that bifurcations with an oscillatory component (Hopf/Flip/Neimark-Sacker) produce in either an increasing or decreasing trend in the lag- $\tau$  autocorrelation function, which depends on the relationship between the lag time and the period of oscillation. By contrast, bifurcations without an oscillatory component (Fold/Transcritical/Pitchfork) only produce an increasing

TABLE I. Tree density on the diamond, square, and linear growth patterns for different burning areas (maximum cluster sizes). Tree densities of three growth patterns were compared for the different system sizes. Bold text indicates the best growth pattern (i.e., maximum tree density).

Maximum cluster size ( $S_{\max}$ )	Tree density ( $\rho$ ) ( $L^2 = 128 \times 128$ )			Tree density ( $\rho$ ) ( $L^2 = 256 \times 256$ )			Tree density ( $\rho$ ) ( $L^2 = 512 \times 512$ )		
	1st <sup>a</sup>	2nd <sup>b</sup>	3rd <sup>c</sup>	1st <sup>a</sup>	2nd <sup>b</sup>	3rd <sup>c</sup>	1st <sup>a</sup>	2nd <sup>b</sup>	3rd <sup>c</sup>
5	<b>0.6270</b>	0.5591	0.5026	<b>0.6260</b>	0.5591	0.5010	<b>0.6255</b>	0.5564	0.5005
9	<b>0.6704</b>	0.6329	0.5071	<b>0.6686</b>	0.6289	0.5020	<b>0.6676</b>	0.6270	0.5011
16	<b>0.6945</b>	0.6857	0.5089	<b>0.6923</b>	0.6857	0.5016	<b>0.6921</b>	0.6809	0.5014
25	0.7151	<b>0.7257</b>	0.5265	0.7161	<b>0.7257</b>	0.5023	0.7158	<b>0.7231</b>	0.5027
36	0.7196	<b>0.7583</b>	0.5233	0.7136	<b>0.7583</b>	0.5026	0.7138	<b>0.7583</b>	0.5020
49	0.7234	<b>0.7931</b>	0.5291	0.7182	<b>0.7871</b>	0.5090	0.7175	<b>0.7842</b>	0.5070
64	0.7179	<b>0.8052</b>	0.5199	0.7198	<b>0.8052</b>	0.5026	0.7145	<b>0.8052</b>	0.5030
...	...	...	...	...	...	...	...	...	...
100	0.7337	<b>0.8301</b>	0.5610	0.7199	<b>0.8238</b>	0.5313	0.7166	<b>0.8206</b>	0.5059
400	0.7593	<b>0.9106</b>	0.7578	0.7484	<b>0.9106</b>	0.6104	0.7251	<b>0.9071</b>	0.5614
900	0.8789	<b>0.9395</b>	0.8789	0.7812	<b>0.9395</b>	0.7812	0.7575	<b>0.9358</b>	0.6386

<sup>a</sup>Diamond growth pattern.

<sup>b</sup>Square growth pattern.

<sup>c</sup>Linear growth pattern.

trend in the lag- $\tau$  autocorrelation function. According to these principles, we conjecture that the forest fire model should be oscillatory bifurcations, while the sandpile model should be nonoscillatory bifurcations. Furthermore, the previous relaxation time is typically obtained by fitting the lag- $\tau$  autocorrelation function with an exponential decay function, but it was only applicable to the case of nonoscillatory bifurcations [15,85,106,107]. Here, our proposed relaxation time is applicable not only to nonoscillatory bifurcations but also to oscillatory bifurcations. A possible explanation for this might be that the lag- $\tau$  autocorrelation function analytical approximation ( $e^{\lambda|\tau|} \cos \omega_0 \tau$ ) [72] has a similar mathematical form to the damped sine wave function ( $A \exp(-\tau/T) \sin[\pi(\tau - \tau_c)/\omega]$ ) in the oscillatory bifurcations. In the other case, the

lag- $\tau$  autocorrelation function analytical approximation ( $e^{\lambda|\tau|}$ ) [72] also has a similar mathematical form to the damped sine wave function in the nonoscillatory bifurcations if the sine function ( $\sin[\pi(\tau - \tau_c)/\omega]$ ) is equal to 1. Here, the relaxation rate ( $\lambda$ ) is defined as the reciprocal of the relaxation time ( $T$ ), i.e.,  $\lambda = 1/T$ . In summary, the relaxation time shows a consistent increasing trend in both oscillatory and nonoscillatory bifurcations when compared to traditional indirect metrics such as the variance and the lag-1 autocorrelation function. This suggests that the relaxation time is a more universal.

Although there are important discoveries revealed by these studies, there are also limitations. On the one hand, constant conditions and spatial homogeneity are assumed in our forest fire model [23]. In the real world, however, fluctuating

TABLE II. The burning area (maximum cluster size) on the diamond, square, linear, and random growth patterns for different tree densities. The burning area of four growth patterns was compared for the different system sizes. Bold text indicates the best growth pattern, which corresponds to the smallest value of the burning area. Unlisted values are less than the value of the next row. For the “4th” columns, 100 independent simulation runs were performed and results represent the mean  $\pm$  standard deviation.

Tree density ( $\rho$ )	Maximum cluster size ( $S_{\max}$ ) ( $L^2 = 128 \times 128$ )				Maximum cluster size ( $S_{\max}$ ) ( $L^2 = 256 \times 256$ )				Maximum cluster size ( $S_{\max}$ ) ( $L^2 = 512 \times 512$ )			
	1st <sup>a</sup>	2nd <sup>b</sup>	3rd <sup>c</sup>	4th <sup>d</sup>	1st <sup>a</sup>	2nd <sup>b</sup>	3rd <sup>c</sup>	4th <sup>d</sup>	1st <sup>a</sup>	2nd <sup>b</sup>	3rd <sup>c</sup>	4th <sup>d</sup>
0.50	1	1	1	248 $\pm$ 55	1	1	1	365 $\pm$ 90	1	1	1	488 $\pm$ 99
0.55		4	81	822 $\pm$ 288		4	81	1442 $\pm$ 43		4	81	2166 $\pm$ 593
0.60	<b>5</b>	9	190	5490 $\pm$ 1527	<b>5</b>	9	190	24212 $\pm$ 4865	<b>5</b>	9	190	103297 $\pm$ 15514
0.65	<b>8</b>	16	237	9877 $\pm$ 216	<b>8</b>	16	237	39993 $\pm$ 357	<b>8</b>	16	237	161070 $\pm$ 618
0.70	<b>13</b>	25	295	11223 $\pm$ 93	<b>13</b>	25	295	44972 $\pm$ 159	<b>13</b>	25	295	180148 $\pm$ 316
0.75	140	<b>36</b>	373	12188 $\pm$ 67	140	<b>36</b>	373	48820 $\pm$ 122	140	<b>36</b>	373	195353 $\pm$ 250
0.80	504	<b>64</b>	505	13075 $\pm$ 54	504	<b>64</b>	505	52289 $\pm$ 115	504	<b>64</b>	505	209227 $\pm$ 236
0.85	698	<b>121</b>	697	13917 $\pm$ 49	698	<b>121</b>	697	55681 $\pm$ 88	698	<b>121</b>	697	222692 $\pm$ 172
0.90	1103	<b>324</b>	1135	14747 $\pm$ 37	1103	<b>324</b>	1135	58993 $\pm$ 75	1103	<b>324</b>	1135	235892 $\pm$ 160

<sup>a</sup>Diamond growth pattern.

<sup>b</sup>Square growth pattern.

<sup>c</sup>Linear growth pattern.

<sup>d</sup>Random growth pattern.

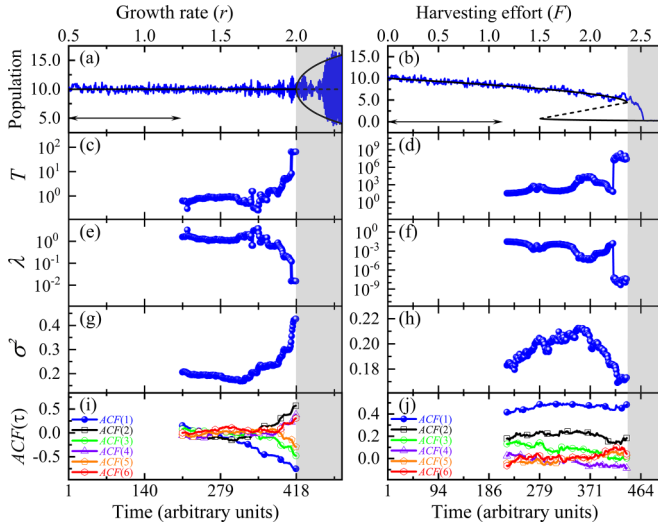


FIG. 7. Characteristic early warning signals preceding the oscillatory and nonoscillatory bifurcations in the Ricker model. (a) Simulated response of population abundance (blue) to increasing growth rate superimposed on Flip bifurcation diagram (black) of the deterministic model (solid, stable state/limit cycle; dashed, unstable state). (b) Simulated response of population abundance (blue) to increasing harvesting effort superimposed on Fold bifurcation diagram (black) of the deterministic model (solid, stable state; dashed, unstable state). Arrow illustrates the rolling window (50% of the time series) used for computing early warning signals. [(c)–(d)] Relaxation time provides an increasing trend in both oscillatory and nonoscillatory bifurcations. [(e)–(f)] Relaxation rate goes to zero as the system approaches bifurcations. (g) Variance provides an increasing trend in the oscillatory bifurcation, but with a weaker rising trend than relaxation time. (h) Variance provides no useful signal in the nonoscillatory bifurcation. (i) The trend of lag- $\tau$  autocorrelation function depends on the lag time for the oscillatory bifurcation. When lag time is an odd number [see blue sphere, green circle, and orange pentagon], it will be a decreasing trend, while when lag time is an even number [see black square, purple triangle, and red hexagon], it will be an increasing trend. (j) The lag- $\tau$  autocorrelation function provides no significant increasing trend for the nonoscillatory bifurcation. The grey band identifies the state after bifurcations, and the parameters of the tipping point are Time = 417 (oscillatory) and Time = 438 (nonoscillatory).

environmental conditions and spatial heterogeneity are considered [108,109]. For instance, the spatial occurrence of most wildfires are not random, since these wildfires are started by people. In the future, we will consider the factors that influence the direction and speed of wildfire spread, including wind, orography, weather, and climate. On the other hand, a number of recent studies have shown that the relaxation time decreases as one approaches the critical point in the conserved Manna sandpile systems [110–112]. A possible explanation for this might be that the conserved systems are the cause of this result. In other words, Dhar and Pradhan *et al.* studied the one-dimensional conserved Manna sandpile systems, whereas we study a two-dimensional nonconserved finite-size sandpile system. Although our work is insufficient to describe the evolution of the real forest fire and sandpile accurately, it provides a viable perspective to predict avalanche events.

Extending the relaxation time into more realistic scenarios with self-organizing systems, such as landslides, earthquakes, and neuronal activity, would be interesting.

As satellite remote sensing technology advances, the increasing availability and resolution of data provide better opportunities to predict the onset of avalanches in self-organizing systems [113]. Existing research uses multiscale satellite data to detect early warning signals of tree mortality in boreal North America [114]. They link these two data sources (i.e., time series of tree-level growth patterns and satellite-based indices) to show that early warning signals of mortality are evident. In the future, we intend to combine these two data sources (i.e., time series data source and spatial snapshot data source) to predict the occurrence of avalanches. How to use spatial snapshot data to estimate the recovery rate is the main challenge currently. To solve this problem, there is an urgent need to develop new indicators based on spatial snapshot data, and this is a goal for future work. In addition, we can also develop more effective early warning signals by using machine learning or deep learning techniques to provide accurate results for preventing the onset of avalanches [115]. Finally, the development and experimental validation of early warning signals for avalanches remains an open research direction.

#### ACKNOWLEDGMENTS

This work was supported by National Natural Science Foundation of China under Grants No. 12265017 and No. 12247205, Yunnan Fundamental Research Projects under Grants No. 202201AV070003 and No. 202101AS070018, Yunnan Ten Thousand Talents Plan Young & Elite Talents Project, Yunnan Province Computational Physics and Applied Science and Technology Innovation Team, National Key R&D Program of China under Grants No. 2021YFA1400900, No. 2021YFA0718300, and No. 2021YFA1402100, NSFC under Grants No. 12174461, No. 12234012, No. 12334012, and No. 52327808, and Space Application System of China Manned Space Program.

#### APPENDIX: CHARACTERISTIC EARLY WARNING SIGNALS PRECEDING THE OSCILLATORY AND NONOSCILLATORY BIFURCATIONS

We illustrate the early warning signals preceding the oscillatory and nonoscillatory bifurcations by using a Ricker-type model that describes the logistic growth of a population subject to harvesting [72,116]. The model is written as follows:

$$N_{t+1} = N_t \exp \left[ r \left( 1 - \frac{N_t}{K} \right) + \sigma \epsilon_t \right] - F \frac{N_t^2}{N_t^2 + h^2}, \quad (\text{A1})$$

where  $N_t$  is the population size at time  $t$ ,  $r$  is the intrinsic growth rate,  $K$  is the carrying capacity,  $F$  is the maximum rate of harvesting,  $h$  is a half-saturation constant,  $\sigma$  is the noise amplitude and  $\epsilon_t$  is a normal random variable with zero mean and unit variance. Baseline parameters are  $r = 0.75$ ,  $K = 10$ ,  $F = 0$ ,  $h = 0.75$ ,  $\sigma = 0.04$ . The model exhibits a Fold bifurcation at  $F = 2.36$ , and a Flip (period-doubling)

bifurcation at  $r = 2.00$  followed by a sequence of further Flip bifurcations to chaos.

We simulate two bifurcation scenarios, namely the oscillatory and nonoscillatory bifurcations. On the one hand, the harvesting rate  $F$  increases linearly over  $[0, 2.7]$ , resulting in a Fold bifurcation. On the other hand, the growth rate  $r$  increases linearly over the interval  $[0.5, 2.3]$  resulting in a Flip bifurcation. Both scenarios are simulated for 500 time steps.

We associate avalanches with a mathematical instability, called bifurcations [78,92,117–120]. The relaxation time as

an indicator for evaluation of bifurcations with oscillations and non-oscillations: an example of Ricker model can be seen in Fig. 7. Compared to conventional indirect metrics such as variance and lag-1 autocorrelation function, the relaxation time can show a consistent with the increasing trend in both oscillatory and nonoscillatory bifurcations, indicating that the relaxation time is more universal. We expect that these findings will stimulate theoretical and experimental work to provide more precise and accurate methods for addressing avalanche events such as forest fires, landslides, and earthquakes in future research.

- 
- [1] R. Sánchez, D. E. Newman, and B. A. Carreras, Waiting-time statistics of self-organized-criticality systems, *Phys. Rev. Lett.* **88**, 068302 (2002).
- [2] B. Drossel, Complex scaling behavior of nonconserved self-organized critical systems, *Phys. Rev. Lett.* **89**, 238701 (2002).
- [3] T.-S. Hsieh, V. A. Lopez, M. H. Black, A. Osinski, K. Pawłowski, D. R. Tomchick, J. Liou, and V. S. Tagliabracchi, Dynamic remodeling of host membranes by self-organizing bacterial effectors, *Science* **372**, 935 (2021).
- [4] T. Misteli, The self-organizing genome: Principles of genome architecture and function, *Cell* **183**, 28 (2020).
- [5] Y. Luo, C. Zeng, and B. Li, Negative rectification and anomalous diffusion in nonlinear substrate potentials: Dynamical relaxation and information entropy, *Phys. Rev. E* **105**, 024204 (2022).
- [6] N. N. Moghadam, F. Nazarimehr, S. Jafari, and J. C. Sprott, Studying the performance of critical slowing down indicators in a biological system with a period-doubling route to chaos, *Physica A* **544**, 123396 (2020).
- [7] J. M. Drake and B. D. Griffen, Early warning signals of extinction in deteriorating environments, *Nature (London)* **467**, 456 (2010).
- [8] V. Dakos, M. Scheffer, E. H. Van Nes, V. Brovkin, V. Petoukhov, and H. Held, Slowing down as an early warning signal for abrupt climate change, *Proc. Natl. Acad. Sci. USA* **105**, 14308 (2008).
- [9] E. H. Van Nes and M. Scheffer, Slow recovery from perturbations as a generic indicator of a nearby catastrophic shift, *Am. Nat.* **169**, 738 (2007).
- [10] C. Wissel, A universal law of the characteristic return time near thresholds, *Oecologia* **65**, 101 (1984).
- [11] B. M. Arani, S. R. Carpenter, L. Lahti, E. H. Van Nes, and M. Scheffer, Exit time as a measure of ecological resilience, *Science* **372**, eaay4895 (2021).
- [12] Z. Ma, Y. Luo, C. Zeng, and B. Zheng, Spatiotemporal diffusion as early warning signal for critical transitions in spatial tumor-immune system with stochasticity, *Phys. Rev. Res.* **4**, 023039 (2022).
- [13] C. Trefois, P. M. Antony, J. Goncalves, A. Skupin, and R. Balling, Critical transitions in chronic disease: Transferring concepts from ecology to systems medicine, *Curr. Opin. Biotechnol.* **34**, 48 (2015).
- [14] B. Spagnolo and A. A. Dubkov, Critical phenomena and diffusion in complex systems, *Int. J. Bifurcation Chaos* **18**, 2643 (2008).
- [15] Z. Ma, C. Zeng, and B. Zheng, Relaxation time as an indicator of critical transition to a eutrophic lake state: The role of stochastic resonance, *Europhys. Lett.* **137**, 42001 (2022).
- [16] P. Ao, D. Galas, L. Hood, L. Yin, and X. Zhu, Towards predictive stochastic dynamical modeling of cancer genesis and progression, *Interdiscip. Sci. Comput. Life Sci.* **2**, 140 (2010).
- [17] S. Field, J. Witt, F. Nori, and X. Ling, Superconducting vortex avalanches, *Phys. Rev. Lett.* **74**, 1206 (1995).
- [18] M. Paczuski, S. Maslov, and P. Bak, Avalanche dynamics in evolution, growth, and depinning models, *Phys. Rev. E* **53**, 414 (1996).
- [19] B. Cerruti and E. Vives, Correlations in avalanche critical points, *Phys. Rev. E* **80**, 011105 (2009).
- [20] C. A. Boulton, T. M. Lenton, and N. Boers, Pronounced loss of amazon rainforest resilience since the early 2000s, *Nat. Clim. Chang.* **12**, 271 (2022).
- [21] C. L. Henley, Statics of a “self-organized” percolation model, *Phys. Rev. Lett.* **71**, 2741 (1993).
- [22] P. Grassberger, Critical behaviour of the Drossel-Schwabl forest fire model, *New J. Phys.* **4**, 17 (2002).
- [23] D. Rybski, V. Butsic, and J. W. Kantelhardt, Self-organized multistability in the forest fire model, *Phys. Rev. E* **104**, L012201 (2021).
- [24] J. Crassous, A. Humeau, S. Boury, and J. Casas, Pressure-dependent friction on granular slopes close to avalanche, *Phys. Rev. Lett.* **119**, 058003 (2017).
- [25] S. Hergarten, Branching with local probability as a paradigm of self-organized criticality, *Phys. Rev. Lett.* **109**, 148001 (2012).
- [26] P. Pradhan and D. Dhar, Probability distribution of residence times of grains in models of rice piles, *Phys. Rev. E* **73**, 021303 (2006).
- [27] S. P. Pudasaini and S. A. Miller, The hypermobility of Huge landslides and avalanches, *Eng. Geol.* **157**, 124 (2013).
- [28] D. K. Keefer, Landslides caused by earthquakes, *Geol. Soc. Am. Bull.* **95**, 406 (1984).
- [29] E. A. Jagla, F. P. Landes, and A. Rosso, Viscoelastic effects in avalanche dynamics: A key to earthquake statistics, *Phys. Rev. Lett.* **112**, 174301 (2014).
- [30] L. W. McFaul, W. J. Wright, X. Gu, J. T. Uhl, and K. A. Dahmen, Aftershocks in slowly compressed bulk metallic glasses: Experiments and theory, *Phys. Rev. E* **97**, 063005 (2018).
- [31] M. J. Aschwanden, N. B. Crosby, M. Dimitropoulou, M. K. Georgoulis, S. Hergarten, J. McAteer, A. V. Milovanov,

- S. Mineshige, L. Morales, N. Nishizuka, G. Pruessner, R. Sanchez, A. S. Sharma, A. Strugarek, and V. Uritsky, 25 years of self-organized criticality: Solar and astrophysics, *Space Sci. Rev.* **198**, 47 (2016).
- [32] G. Boffetta, V. Carbone, P. Giuliani, P. Veltri, and A. Vulpiani, Power laws in solar flares: Self-organized criticality or turbulence?, *Phys. Rev. Lett.* **83**, 4662 (1999).
- [33] M. Paczuski, S. Boettcher, and M. Baiesi, Interoccurrence times in the Bak-Tang-Wiesenfeld sandpile model: A comparison with the observed statistics of solar flares, *Phys. Rev. Lett.* **95**, 181102 (2005).
- [34] F. Y. Kalle Kossio, S. Goedeke, B. van den Akker, B. Ibarz, and R.-M. Memmesheimer, Growing critical: Self-organized criticality in a developing neural system, *Phys. Rev. Lett.* **121**, 058301 (2018).
- [35] L. de Arcangelis, C. Perrone-Capano, and H. J. Herrmann, Self-organized criticality model for brain plasticity, *Phys. Rev. Lett.* **96**, 028107 (2006).
- [36] N. J. Abram, B. J. Henley, A. Sen Gupta, T. J. Lippmann, H. Clarke, A. J. Dowdy, J. J. Sharples, R. H. Nolan, T. Zhang, M. J. Wooster *et al.*, Connections of climate change and variability to large and extreme forest fires in southeast australia, *Commun. Earth Environ.* **2**, 8 (2021).
- [37] D. M. Bowman, G. J. Williamson, R. K. Gibson, R. A. Bradstock, and R. J. Keenan, The severity and extent of the Australia 2019–20 Eucalyptus forest fires are not the legacy of forest management, *Nat. Ecol. Evol.* **5**, 1003 (2021).
- [38] M. M. Boer, V. Resco de Dios, and R. A. Bradstock, Unprecedented burn area of Australian mega forest fires, *Nat. Clim. Chang.* **10**, 171 (2020).
- [39] H. L. D. de S. Cavalcante, M. Oriá, D. Sornette, E. Ott, and D. J. Gauthier, Predictability and suppression of extreme events in a chaotic system, *Phys. Rev. Lett.* **111**, 198701 (2013).
- [40] K. Klocke, T. M. Wintermantel, G. Lohead, S. Whitlock, and M. Buchhold, Hydrodynamic stabilization of self-organized criticality in a driven Rydberg gas, *Phys. Rev. Lett.* **126**, 123401 (2021).
- [41] J. Rosendahl, M. Vekić, and J. E. Rutledge, Predictability of large avalanches on a sandpile, *Phys. Rev. Lett.* **73**, 537 (1994).
- [42] O. Ramos, E. Altshuler, and K. J. Måløy, Avalanche prediction in a self-organized pile of beads, *Phys. Rev. Lett.* **102**, 078701 (2009).
- [43] J. Rajchenbach, Dynamics of grain avalanches, *Phys. Rev. Lett.* **88**, 014301 (2001).
- [44] P. Bak, *How Nature works: The Science of Self-Organized Criticality* (Springer Science & Business Media, New York, 1996).
- [45] F. Caruso, A. Pluchino, V. Latora, S. Vinciguerra, and A. Rapisarda, Analysis of self-organized criticality in the Olami-Feder-Christensen model and in real earthquakes, *Phys. Rev. E* **75**, 055101(R) (2007).
- [46] P. Bak, C. Tang, and K. Wiesenfeld, Self-organized criticality: An explanation of the  $1/f$  noise, *Phys. Rev. Lett.* **59**, 381 (1987).
- [47] P. Bak, C. Tang, and K. Wiesenfeld, Self-organized criticality, *Phys. Rev. A* **38**, 364 (1988).
- [48] G. Pruessner, *Self-Organised Criticality: Theory, Models and Characterisation* (Cambridge University Press, Cambridge, 2012).
- [49] R. J. Geller, D. D. Jackson, Y. Y. Kagan, and F. Mulargia, Earthquakes cannot be predicted, *Science* **275**, 1616 (1997).
- [50] X. Yang, S. Du, and J. Ma, Do earthquakes exhibit self-organized criticality? *Phys. Rev. Lett.* **92**, 228501 (2004).
- [51] J. Davidsen and A. Green, Are earthquake magnitudes clustered? *Phys. Rev. Lett.* **106**, 108502 (2011).
- [52] O. Ramos, Criticality in earthquakes. Good or bad for prediction? *Tectonophysics* **485**, 321 (2010).
- [53] A. Corral, L. Telesca, and R. Lasaponara, Scaling and correlations in the dynamics of forest-fire occurrence, *Phys. Rev. E* **77**, 016101 (2008).
- [54] L. Telesca, G. Amatulli, R. Lasaponara, M. Lovallo, and A. Santulli, Time-scaling properties in forest-fire sequences observed in Gargano area (southern italy), *Ecol. Model.* **185**, 531 (2005).
- [55] J.-D. Bancal and R. Pastor-Satorras, Steady-state dynamics of the forest fire model on complex networks, *Eur. Phys. J. B* **76**, 109 (2010).
- [56] J. S. Clark, S. R. Carpenter, M. Barber, S. Collins, A. Dobson, J. A. Foley, D. M. Lodge, M. Pascual, R. Pielke, Jr., W. Pizer *et al.*, Ecological forecasts: An emerging imperative, *Science* **293**, 657 (2001).
- [57] D. Ludwig, Is it meaningful to estimate a probability of extinction? *Ecology* **80**, 298 (1999).
- [58] S. Lise and M. Paczuski, Nonconservative earthquake model of self-organized criticality on a random graph, *Phys. Rev. Lett.* **88**, 228301 (2002).
- [59] B. Drossel and F. Schwabl, Self-organized critical forest-fire model, *Phys. Rev. Lett.* **69**, 1629 (1992).
- [60] M. Joglekar, E. Ott, and J. A. Yorke, Scaling of chaos versus periodicity: How certain is it that an attractor is chaotic? *Phys. Rev. Lett.* **113**, 084101 (2014).
- [61] H.-J. Zhu, K. Xu, G.-F. Zhang, and W.-M. Liu, Finite-component multicriticality at the superradiant quantum phase transition, *Phys. Rev. Lett.* **125**, 050402 (2020).
- [62] D. Dhar, Self-organized critical state of sandpile automaton models, *Phys. Rev. Lett.* **64**, 1613 (1990).
- [63] D. Dhar and R. Ramaswamy, Exactly solved model of self-organized critical phenomena, *Phys. Rev. Lett.* **63**, 1659 (1989).
- [64] T. Hutchcroft, New critical exponent inequalities for percolation and the random cluster model, *Probability and Mathematical Physics* **1**, 147 (2020).
- [65] G. Todorova and B. Yordanov, Critical exponent for a nonlinear wave equation with damping, *J. Differ. Equ.* **174**, 464 (2001).
- [66] F. D. Schneider and S. Kéfi, Spatially heterogeneous pressure raises risk of catastrophic shifts, *Theor. Ecol.* **9**, 207 (2016).
- [67] S. di Santo, R. Burioni, A. Vezzani, and M. A. Muñoz, Self-organized bistability associated with first-order phase transitions, *Phys. Rev. Lett.* **116**, 240601 (2016).
- [68] S. Kéfi, M. Rietkerk, M. Roy, A. Franc, P. C. De Ruiter, and M. Pascual, Robust scaling in ecosystems and the meltdown of patch size distributions before extinction, *Ecol. Lett.* **14**, 29 (2011).
- [69] G. Forzieri, V. Dakos, N. G. McDowell, A. Ramdane, and A. Cescatti, Emerging signals of declining forest resilience under climate change, *Nature (London)* **608**, 534 (2022).
- [70] A. J. Veraart, E. J. Faassen, V. Dakos, E. H. Van Nes, M. Lürling, and M. Scheffer, Recovery rates reflect distance to

- a tipping point in a living system, *Nature (London)* **481**, 357 (2012).
- [71] I. A. van de Leemput, M. Wichers, A. O. Cramer, D. Borsboom, F. Tuerlinckx, P. Kuppens, E. H. Van Nes, W. Viechtbauer, E. J. Giltay, S. H. Aggen *et al.*, Critical slowing down as early warning for the onset and termination of depression, *Proc. Natl. Acad. Sci. USA* **111**, 87 (2014).
- [72] T. M. Bury, C. T. Bauch, and M. Anand, Detecting and distinguishing tipping points using spectral early warning signals, *J. R. Soc. Interface* **17**, 20200482 (2020).
- [73] P. E. McSharry, L. A. Smith, and L. Tarassenko, Prediction of epileptic seizures: Are nonlinear methods relevant? *Nat. Med.* **9**, 241 (2003).
- [74] S. R. Carpenter and W. A. Brock, Rising variance: A leading indicator of ecological transition, *Ecol. Lett.* **9**, 311 (2006).
- [75] V. Dakos, S. R. Carpenter, W. A. Brock, A. M. Ellison, V. Guttal, A. R. Ives, S. Kéfi, V. Livina, D. A. Seekell, E. H. van Nes *et al.*, Methods for detecting early warnings of critical transitions in time series illustrated using simulated ecological data, *PLoS ONE* **7**, e41010 (2012).
- [76] Y. Sharma, P. S. Dutta, and A. K. Gupta, Anticipating regime shifts in gene expression: The case of an autoactivating positive feedback loop, *Phys. Rev. E* **93**, 032404 (2016).
- [77] S. Orozco-Fuentes, G. Griffiths, M. Holmes, R. Ettelaie, J. Smith, A. Baggaley, and N. Parker, Early warning signals in plant disease outbreaks, *Ecol. Model.* **393**, 12 (2019).
- [78] M. Scheffer, J. Bascompte, W. A. Brock, V. Brovkin, S. R. Carpenter, V. Dakos, H. Held, E. H. Van Nes, M. Rietkerk, and G. Sugihara, Early-warning signals for critical transitions, *Nature (London)* **461**, 53 (2009).
- [79] V. Dakos, E. H. van Nes, P. D'Odorico, and M. Scheffer, Robustness of variance and autocorrelation as indicators of critical slowing down, *Ecology* **93**, 264 (2012).
- [80] S. R. Carpenter, J. J. Cole, M. L. Pace, R. Batt, W. A. Brock, T. Cline, J. Coloso, J. R. Hodgson, J. F. Kitchell, D. A. Seekell *et al.*, Early warnings of regime shifts: A whole-ecosystem experiment, *Science* **332**, 1079 (2011).
- [81] L. Dai, D. Vorselen, K. S. Korolev, and J. Gore, Generic indicators for loss of resilience before a tipping point leading to population collapse, *Science* **336**, 1175 (2012).
- [82] V. Dakos, S. Kéfi, M. Rietkerk, E. H. Van Nes, and M. Scheffer, Slowing down in spatially patterned ecosystems at the brink of collapse, *Am. Nat.* **177**, E153 (2011).
- [83] M. Scheffer, S. R. Carpenter, V. Dakos, and E. H. van Nes, Generic indicators of ecological resilience: Inferring the chance of a critical transition, *Annu. Rev. Ecol. Syst.* **46**, 145 (2015).
- [84] S. Kéfi, V. Guttal, W. A. Brock, S. R. Carpenter, A. M. Ellison, V. N. Livina, D. A. Seekell, M. Scheffer, E. H. van Nes, and V. Dakos, Early warning signals of ecological transitions: methods for spatial patterns, *PLoS ONE* **9**, e92097 (2014).
- [85] R. C. Löffler, T. Bäuerle, M. Kardar, C. M. Rohwer, and C. Bechinger, Behavior-dependent critical dynamics in collective states of active particles, *Europhys. Lett.* **134**, 64001 (2021).
- [86] R. M. Rizk-Allah and A. E. Hassani, A movable damped wave algorithm for solving global optimization problems, *Evol. Intel.* **12**, 49 (2019).
- [87] R. M. May, Thresholds and breakpoints in ecosystems with a multiplicity of stable states, *Nature (London)* **269**, 471 (1977).
- [88] C. S. Holling, Resilience and stability of ecological systems, *Annu. Rev. Ecol. Syst.* **4**, 1 (1973).
- [89] F. Dablander, A. Pichler, A. Cika, and A. Bacilieri, Anticipating critical transitions in psychological systems using early warning signals: Theoretical and practical considerations., *Psychol. Methods* **28**, 765 (2022).
- [90] O. Ramos, E. Altshuler, and K. J. Måløy, Quasiperiodic events in an earthquake model, *Phys. Rev. Lett.* **96**, 098501 (2006).
- [91] S.-J. Wang, G. Ouyang, J. Guang, M. Zhang, K. Y. Michael Wong, and C. Zhou, Stochastic oscillation in self-organized critical states of small systems: Sensitive resting state in neural systems, *Phys. Rev. Lett.* **116**, 018101 (2016).
- [92] T. Quail, A. Shrier, and L. Glass, Predicting the onset of period-doubling bifurcations in noisy cardiac systems, *Proc. Natl. Acad. Sci. USA* **112**, 9358 (2015).
- [93] J. Fan, J. Meng, J. Ludescher, X. Chen, Y. Ashkenazy, J. Kurths, S. Havlin, and H. J. Schellnhuber, Statistical physics approaches to the complex earth system, *Phys. Rep.* **896**, 1 (2021).
- [94] T. Kleinen, H. Held, and G. Petschel-Held, The potential role of spectral properties in detecting thresholds in the earth system: Application to the thermohaline circulation, *Ocean Dyn.* **53**, 53 (2003).
- [95] V. N. Livina and T. M. Lenton, A modified method for detecting incipient bifurcations in a dynamical system, *Geophys. Res. Lett.* **34**, 2006GL028672 (2007).
- [96] S. H. Strogatz, *Nonlinear Dynamics and Chaos: With Applications to Physics, Biology, Chemistry, and Engineering*, 2nd ed. (CRC Press, Boca Raton, FL, 2015), p. 532.
- [97] R. D. Zinck and V. Grimm, Unifying wildfire models from ecology and statistical physics, *Am. Natural.* **174**, E170 (2009).
- [98] S. Lübeck and K. D. Usadel, Numerical determination of the avalanche exponents of the Bak-Tang-Wiesenfeld model, *Phys. Rev. E* **55**, 4095 (1997).
- [99] D. V. Kitanov, S. Lübeck, P. Grassberger, and V. B. Priezzhev, Scaling of waves in the Bak-Tang-Wiesenfeld sandpile model, *Phys. Rev. E* **61**, 81 (2000).
- [100] P. Pradhan, Time-dependent properties of sandpiles, *Front. Phys.* **9**, 641233 (2021).
- [101] D. Stauffer and A. Aharony, *Introduction To Percolation Theory: Second Edition*, 2nd ed. (Taylor & Francis, London, 1992).
- [102] A. Bunde and S. Havlin, Percolation i, in *Fractals and Disordered Systems*, edited by A. Bunde and S. Havlin (Springer, Berlin, 1996), pp. 59–114.
- [103] S. I. Pak and T. Hayakawa, Forest fire modeling using cellular automata and percolation threshold analysis, in *Proceedings of the 2011 American Control Conference* (IEEE, San Francisco, CA, USA, 2011), pp. 293–298.
- [104] N. J. Nagelkerke *et al.*, A note on a general definition of the coefficient of determination, *Biometrika* **78**, 691 (1991).
- [105] D. Chicco, M. J. Warrens, and G. Jurman, The coefficient of determination R-squared is more informative than SMAPE, MAE, MAPE, MSE, and RMSE in regression analysis evaluation, *Peer J. Comput. Sci.* **7**, e623 (2021).
- [106] D. B. Brückner, H. Chen, L. Barinov, B. Zoller, and T. Gregor, Stochastic motion and transcriptional dynamics of pairs of

- distal dna loci on a compacted chromosome, *Science* **380**, 1357 (2023).
- [107] A. V. Savin, G. P. Tsironis, and X. Zotos, Thermal conductivity of a classical one-dimensional spin-phonon system, *Phys. Rev. B* **75**, 214305 (2007).
- [108] M. A. Moritz, E. Batllori, R. A. Bradstock, A. M. Gill, J. Handmer, P. F. Hessburg, J. Leonard, S. McCaffrey, D. C. Odion, T. Schoennagel *et al.*, Learning to coexist with wildfire, *Nature (London)* **515**, 58 (2014).
- [109] M. A. Krawchuk, M. A. Moritz, M.-A. Parisien, J. Van Dorn, and K. Hayhoe, Global pyrogeography: The current and future distribution of wildfire, *PLoS ONE* **4**, e5102 (2009).
- [110] A. Mukherjee and P. Pradhan, Dynamic correlations in the conserved manna sandpile, *Phys. Rev. E* **107**, 024109 (2023).
- [111] D. Tapader, P. Pradhan, and D. Dhar, Density relaxation in conserved manna sandpiles, *Phys. Rev. E* **103**, 032122 (2021).
- [112] S. Chatterjee, A. Das, and P. Pradhan, Hydrodynamics, density fluctuations, and universality in conserved stochastic sandpiles, *Phys. Rev. E* **97**, 062142 (2018).
- [113] E. Babaeian, M. Sadeghi, S. B. Jones, C. Montzka, H. Vereecken, and M. Tuller, Ground, proximal, and satellite remote sensing of soil moisture, *Rev. Geophys.* **57**, 530 (2019).
- [114] B. M. Rogers, K. Solvik, E. H. Hogg, J. Ju, J. G. Masek, M. Michaelian, L. T. Berner, and S. J. Goetz, Detecting early warning signals of tree mortality in boreal North America using multiscale satellite data, *Global Change Biol.* **24**, 2284 (2018).
- [115] T. M. Bury, D. Dylewsky, C. T. Bauch, M. Anand, L. Glass, A. Shrier, and G. Bub, Predicting discrete-time bifurcations with deep learning, *Nat. Commun.* **14**, 6331 (2023).
- [116] V. Dakos, S. M. Glaser, C.-H. Hsieh, and G. Sugihara, Elevated nonlinearity as an indicator of shifts in the dynamics of populations under stress, *J. R. Soc. Interface* **14**, 20160845 (2017).
- [117] F. Pittorino, M. Ibáñez-Berganza, M. di Volo, A. Vezzani, and R. Burioni, Chaos and correlated avalanches in excitatory neural networks with synaptic plasticity, *Phys. Rev. Lett.* **118**, 098102 (2017).
- [118] M. W. Adamson, J. H. Dawes, A. Hastings, and F. M. Hilker, Forecasting resilience profiles of the run-up to regime shifts in nearly-one-dimensional systems, *J. R. Soc. Interface* **17**, 20200566 (2020).
- [119] T. M. Bury, R. Sujith, I. Pavithran, M. Scheffer, T. M. Lenton, M. Anand, and C. T. Bauch, Deep learning for early warning signals of tipping points, *Proc. Natl. Acad. Sci. USA* **118**, e2106140118 (2021).
- [120] Y.-C. Chen, C. Shi, J. M. Kosterlitz, X. Zhu, and P. Ao, Topology, vorticity, and limit cycle in a stabilized Kuramoto-Sivashinsky equation, *Proc. Natl. Acad. Sci. USA* **119**, e2211359119 (2022).